Models of crack propagation. II. Two-dimensional model with dissipation on the fracture surface

J. S. Langer

Institute for Theoretical Physics, University of California, Santa Barbara, Santa Barbara, California 93106-4030

Hiizu Nakanishi

Department of Physics, Faculty of Science and Technology, Keio University, Yokohama 223, Japan
(Received 4 March 1993)

We discuss a model of steady-state crack propagation in a two-dimensional material whose displacements obey a massive scalar wave equation. The tractions on the fracture surface consist of a conventional cohesive stress plus a viscous dissipation. Much of the paper is devoted to the development of Wiener-Hopf methods for an analysis of this model. The most notable result is that, when the dissipation is sufficiently strong, the crack creeps very slowly at external stresses just above the Griffith threshold, and makes an abrupt transition to propagation at roughly the Rayleigh wave speed at higher stresses. Thus the model exhibits a dissipation-dependent effective threshold for fracture.

I. INTRODUCTION

This paper is the third in a series [1,2] of studies of rudimentary models of steady-state crack propagation. The general strategy in these studies has been to compute propagation speeds as functions of externally applied stress and various constitutive properties of the models. The particular model to be investigated here is two dimensional, thus it contains the long-range interactions and stress concentrations that are essential to a realistic theory of cracks moving in elastic materials [3].

The crucial ingredient of this model is a simple mechanism for dissipation of energy on the crack surface. We shall see that this mechanism causes the motion of the crack to change very abruptly from slow creep at small applied stresses to propagation at nearly the Rayleigh wave speed at higher stresses. The transition occurs at an applied stress that may be appreciably greater than the Griffith threshold [4]. The appearance of such a transition as an intrinsically dynamic feature of this model raises interesting questions about some basic elements of fracture theory. For example, the results to be described here may provide new understanding of what we mean by fracture toughness or how we distinguish between the dynamic properties of cracks in brittle versus ductile materials. Our main purpose in the present paper, however, is to present a systematic and reasonably complete account of the mathematics and physics of this model. More speculative interpretations and extensions are left for other publications.

A major part of the work to be described here is analytic; indeed, a secondary purpose of this investigation has been to develop mathematical tools for dealing with problems of this kind. Modern computational techniques have made it relatively easy to carry out fully dynamic numerical experiments using these models, and such work is being done as part of the present project. But numerical experiments on their own generally do not lead to full understanding of the underlying physical principles; they are most useful when supplemented by exact mathematical results whenever such results are obtainable. It is in that spirit that we present the following analysis.

II. SPECIFICS OF THE MODEL

Consider a semi-finite elastic material occupying the upper half of the x, y plane ($y > 0$), and suppose that a mode-III (antiplane) crack moves along the x axis. (Alternatively, we may visualize the system as occupying the entire plane, the lower half being the reflection of the upper.) The displacement of the material, $u(x,y,t)$, obeys a scalar, massive wave equation of the form

$$\ddot{u} = c_0^2 \nabla^2 u - \omega_0^2 (u - \Delta) . \tag{2.1}$$

Here, c_0 is the wave speed, ω_0 is the "mass," and $\omega_0^2 \Delta$ is an applied force. As in previous work [2,5], we include the mass in (2.1) as a device that allows us to consider a finite applied strain without having to deal explicitly with the outer boundaries of the system. In effect, our material is tied elastically to a substrate or, within a reasonable approximation, the crack is moving along the center line of a strip of finite width. The presence of a small but nonzero ω_0 in (2.1) implies the existence of a large length scale in the system, for example, the width of the strip or the distance between the material and the substrate. By definition, $u = 0$ along the unbroken portion of the x axis. Far from this axis, or well behind the crack tip where the cohesive forces vanish and the stress is fully relaxed, the displacement u relaxes to Δ. Note that, unlike in previous papers [1,2], there is no dissipative term in (2.1).

To complete the definition of the model, we must specify the tractions to be applied to the fracture surface. The crucial assumption is that these tractions can be written in the form

$$\mu \frac{\partial u}{\partial y}\bigg|_{y=0} = \begin{cases} \sigma(x), & u(x,0,t)=0 \\ \sigma_c\{u\} - \eta \dfrac{\partial^2 \dot{u}}{\partial x^2}\bigg|_{y=0}, & u(x,0,t)>0 . \end{cases} \quad (2.2)$$

The quantity μ on the left-hand side of (2.2) is an elastic modulus. On the right-hand side, $\sigma(x)$ is an unknown stress acting across the fracture line ahead of the crack tip, where $u=0$. Behind the crack tip, where $u>0$, the function $\sigma_c\{u(x,0,t)\}$ is the cohesive stress acting between the open crack faces. For example, we shall use

$$\sigma_c\{u\} = \begin{cases} \sigma_y, & 0<u<\delta \\ 0, & u>\delta, \end{cases} \quad (2.3)$$

where σ_y is the yield stress and δ is the range of the cohesive force. This simple picture of the Barenblatt [6] cohesive zone is convenient for analytic purposes. None of the qualitative features of the results to be presented here are likely to depend on the details of this picture and, in fact, all of the results in Secs. III–VI will be independent of any specific assumptions about $\sigma_c\{u\}$.

The second term on the right-hand side of (2.2) is a viscous damping stress acting on the fracture surface. A viscosity of this form appears in a one-dimensional model in Ref. [2], and we recently have used it in a one-dimensional model of rupture on an earthquake fault [7]. In the latter case, a velocity-weakening, stick-slip friction law produces shocklike rupture pulses [5], and the viscosity is necessary in order to regularize the otherwise singular behavior of these pulses. One of the motivations for the present work is the need to generalize the rupture model to two-dimensional systems. At present, however, we shall consider the viscous model only for the case of simple fracture, where the stress σ_c contains a cohesive force but no stick-slip friction, and the crack faces remain permanently disengaged from each other after the crack has opened.

We should think of the viscosity η as being no more than a phenomenological parameter at this stage of the inquiry. There is no a priori reason why such a term should not be present in (2.2); it is not forbidden by any conservation law or symmetry principle; and it is manifestly the simplest way to introduce a localized dissipative mechanism without adding more than a single new length scale to the problem. The two spatial derivatives preserve reflection and translation symmetries, and the single time derivative breaks time-reversal symmetry to produce energy dissipation. There are infinitely many more complicated ways of doing this. More realistic dissipative terms are likely to be nonlinear or, at the very least, η would be some strain-rate-dependent, nonlocal operator. But explicitly nonlocal interactions necessarily would introduce extra length scales. Those new length scales might turn out to be significant when the underlying physical mechanisms are better understood, but they would produce unnecessary complexity at this stage of the investigation.

Without loss of generality, we may set both c_0 and ω_0 equal to unity in (2.1) by making the transformations $\omega_0 t \to t$ and $\omega_0 x /c_0 \to x$, $\omega_0 y /c_0 \to y$. This means that we are measuring spatial distances in units of the macroscopic length scale in the system, $W \equiv c_0 /\omega_0$. For present purposes, it is most convenient to use the same units for the displacement u as those that we are using for x and y, that is, $\omega_0 u /c_0 = u /W \to u$, and $\Delta /W = \varepsilon_\infty$ is the externally applied strain. Thus (2.1) becomes

$$\ddot{u} = \nabla^2 u - u + \varepsilon_\infty \quad (2.4)$$

and (2.2), after division by μ, becomes

$$\frac{\partial u}{\partial y}\bigg|_{y=0} = \begin{cases} \varepsilon(x), & u(x,0,t)=0 \\ \varepsilon_c\{u\} - \tilde{\eta} \dfrac{\partial^2 \dot{u}}{\partial x^2}\bigg|_{y=0}, & u(x,0,t)>0 . \end{cases} \quad (2.5)$$

Here, $\varepsilon(x)=\sigma(x)/\mu$, $\varepsilon_c\{u\}=\sigma_c\{u\}/\mu$, and $\tilde{\eta}=\omega_0^2\eta/\mu c_0$. Note that $\tilde{\eta}$ scales as W^{-2} and will be very small for most cases of interest. On the other hand, $\tilde{\eta}$ multiplies the highest derivative in these equations and therefore will play a controlling role in the analysis.

III. WIENER-HOPF SOLUTIONS

We look for steady-state solutions of (2.4) and (2.5) in a frame of reference moving at speed $-v$; thus we write $u(x,y,t)=\bar{u}(x+vt,y)$. For subsonic velocities, $v<1$, it is convenient to denote $\bar{u}(x+vt,0)=U(\xi)$, where $\beta\xi=x+vt$ and $\beta^2=1-v^2$. (We shall consider supersonic motion in Sec. VI.) The tip of the crack is at $\xi=0$; thus $U(\xi)=0$ for $\xi<0$.

The Wiener-Hopf method for solving problems of this kind starts with the Fourier representation of $\bar{u}$:

$$\bar{u}(x+vt,y)=\varepsilon_\infty(1-e^{-y})+ \int \frac{dk}{2\pi} \hat{U}^{(+)}(k)e^{ik\xi - \hat{K}y} . \quad (3.1)$$

The first term on the right-hand side is the uniformly stressed state of the system in the absence of a crack, and the second term is the perturbation caused by the crack. $\hat{U}^{(+)}(k)$ is the Fourier transform of $U(\xi)$. From (2.4) we know that

$$\hat{K}(k)=(k^2+1)^{1/2}, \quad \mathrm{Re}\hat{K} \geq 0 . \quad (3.2)$$

The superscript $(+)$ in the expression $\hat{U}^{(+)}(k)$ means that this function has singularities only in the upper half k plane, that is, it is the Fourier transform of the function $U(\xi)$, which is nonzero only for positive ξ. The superscript $(-)$ will have the obvious opposite meaning. (This notation is reversed from that used in Refs. [1,2].)

The Fourier transform of (2.5), after some rearrangement, can be written in the form

$$-\hat{Q}(k)ik\hat{U}^{(+)}(k)=ik\hat{\varepsilon}^{(-)}(k)+ik\hat{\varepsilon}_c^{(+)}(k)-\varepsilon_\infty , \quad (3.3)$$

where

$$\hat{Q}(k)=(k^2+1)^{1/2}+i\nu k^3 , \quad (3.4)$$

$$\hat{\varepsilon}^{(-)}(k)= \int_{-\infty}^0 d\xi \, e^{-ik\xi}[\bar{\varepsilon}(\xi)-\varepsilon_\infty] , \quad (3.5)$$

$$\hat{\varepsilon}_c^{(+)}(k)= \int_0^\infty d\xi \, e^{-ik\xi}\varepsilon_c\{U(\xi)\} , \quad (3.6)$$

and $\bar{\varepsilon}(\xi)=\varepsilon(x)$. In (3.4) we have introduced the group of parameters $\nu=\bar{\eta}v/\beta^3$, which will play an important role in our analysis. The Wiener-Hopf strategy is to write $\hat{Q}(k)$ as the product $\hat{Q}^{(+)}(k)\hat{Q}^{(-)}(k)$ so that (3.3) can be further rearranged to read

$$\hat{Q}^{(+)}(k)ik\hat{U}^{(+)}(k)+ik\hat{\Lambda}^{(+)}(k)$$

$$=\frac{1}{\hat{Q}^{(-)}(k)}[\varepsilon_\infty-ik\hat{\varepsilon}^{(-)}(k)]-ik\hat{\Lambda}^{(-)}(k) \ . \quad (3.7)$$

Here,

$$\hat{\Lambda}^{(\pm)}(k)=\mp\int_{C(\pm)}\frac{dk'}{2\pi i}\frac{1}{(k'-k)}\frac{\hat{\varepsilon}_c^{(+)}(k')}{\hat{Q}^{(-)}(k')} \ , \quad (3.8)$$

where the contours $C^{(+)}$ and $C^{(-)}$ go from $-\infty$ to $+\infty$ in the k' plane passing, respectively, above and below the pole at $k'=k$.

Both sides of (3.7) must be equal to the same entire function of k which, in this case, we may take to be a constant, say A. Evaluating both sides in the limit $k\rightarrow 0$, and using $\lim_{k\rightarrow 0}ik\hat{U}^{(+)}(k)=U(\infty)$, we find

$$A=\hat{Q}^{(+)}(0)U(\infty)=\frac{\varepsilon_\infty}{\hat{Q}^{(-)}(0)} \ . \quad (3.9)$$

This result depends on the fact that both $\hat{\varepsilon}_c^{(+)}(k)$ and $\hat{\varepsilon}^{(-)}(k)$ are regular at $k=0$ which, in turn, is because $\varepsilon_c\{U(\xi)\}$ vanishes at $\xi\rightarrow+\infty$ in the integrand in (3.6) and $\bar{\varepsilon}(\xi)-\varepsilon_\infty$ vanishes at $\xi\rightarrow-\infty$ in (3.5). Note that, from (3.4), $\hat{Q}(0)=\hat{Q}^{(+)}(0)\hat{Q}^{(-)}(0)=1$; thus (3.9) assures us that our solution satisfies $U(\infty)=\varepsilon_\infty$. Without loss of generality, we may normalize the factors $\hat{Q}^{(\pm)}(k)$ so that $\hat{Q}^{(+)}(0)=\hat{Q}^{(-)}(0)=1$.

Our formal solution is now the following. For the crack-opening displacement

$$ik\hat{U}^{(+)}(k)=\frac{1}{\hat{Q}^{(+)}(k)}[\varepsilon_\infty-ik\hat{\Lambda}^{(+)}(k)] \ . \quad (3.10)$$

For the unknown stress ahead of the crack tip

$$ik\hat{\varepsilon}^{(-)}(k)=\varepsilon_\infty[1-\hat{Q}^{(-)}(k)]-ik\hat{Q}^{(-)}(k)\hat{\Lambda}^{(-)}(k) \ . \quad (3.11)$$

IV. EVALUATION OF THE WIENER-HOPF SOLUTIONS

The various expressions appearing in (3.10) and (3.11) must be evaluated and transformed into functions of ξ before they will be useful for physical interpretation. The first step in this process is to compute the factors $\hat{Q}^{(\pm)}(k)$.

The function $\hat{Q}(k)$ clearly has branch points at $k=\pm i$ and, in order that $\text{Re}\hat{K}(k)\geq 0$ as required by (3.2), the associated branch cuts may be chosen to run from $+i$ to $+i\infty$ and from $-i$ to $-i\infty$. Closer inspection of (3.4) reveals that $\hat{Q}(k)$ has three zeros on the physical sheet of the complex k plane at, say, $k=k_0$, k_1, and k_2. The root $k_0\equiv-ip_0$ is always on the negative imaginary k axis; k_1 is complex with positive real and imaginary parts; $k_2=-k_1^*$; and $-i\nu k_0k_1k_2=+1$. For $\nu\ll 1$

$$p_0\approx 1-\frac{\nu^2}{2}+\cdots \quad (4.1)$$

and

$$k_1\approx\left[\frac{i}{\nu}\right]^{1/2} \ . \quad (4.2)$$

We factor $\hat{Q}(k)$ by using the Cauchy method to write

$$\ln\left[\frac{\hat{Q}(k)}{i\nu(k-k_0)(k-k_1)(k-k_2)}\right]=\Phi^{(+)}(k)+\Phi^{(-)}(k) \ . \quad (4.3)$$

Because the only singularities of function on the left-hand side of (4.3) are the branch points at $\pm i$, the $\Phi^{(\pm)}$ can be expressed as integrals over the discontinuities across the corresponding branch cuts:

$$\Phi^{(\pm)}(k)=\mp\int_1^\infty\frac{dp}{\pi}\frac{\theta(p)}{(p\pm ik)} \ , \quad (4.4)$$

where

$$\theta(p)=\arctan\left[\frac{\sqrt{p^2-1}}{\nu p^3}\right] \ . \quad (4.5)$$

We now can write the $\hat{Q}^{(\pm)}$ in the form

$$\hat{Q}^{(+)}(k)=-i\nu k_0(k-k_1)(k-k_2)$$
$$\times\exp[\Phi^{(+)}(k)-\Phi^{(+)}(0)] \ , \quad (4.6)$$

$$\hat{Q}^{(-)}(k)=\left[1-\frac{k}{k_0}\right]\exp[\Phi^{(-)}(k)-\Phi^{(-)}(0)] \ . \quad (4.7)$$

The crucial role played by the parameter $\bar{\eta}$ is immediately apparent in these results. When $\nu=\bar{\eta}v/\beta^3$ vanishes, k_1 and k_2 move off to infinity and, most importantly, $\theta(p)$ remains equal to $\pi/2$ for $p\rightarrow\infty$. We obtain the required limit, $\hat{Q}^{(\pm)}\rightarrow(k\mp i)^{1/2}$, but only because indefinitely large contributions to $\Phi^{(\pm)}$ in (4.4) cancel one another in (4.3). On the other hand, so long as ν is nonzero, $\theta(p)$ vanishes as p^{-2} for large p, that is, for $p\gg\nu^{-1/2}\approx|k_1|$; and the discontinuities across the cuts in $\Phi^{(\pm)}(k)$ vanish at large k. In particular,

$$\Phi^{(\pm)}(k\rightarrow\infty)\approx\frac{ip_\infty}{k} \ , \quad (4.8)$$

where

$$p_\infty=\frac{1}{\pi}\int_1^\infty dq\arctan\left[\frac{\sqrt{q^2-1}}{\nu q^3}\right] \ . \quad (4.9)$$

This major modification of the structure of the Wiener-Hopf kernel at large k implies equally major modifications of $U(\xi)$ and $\bar{\varepsilon}(\xi)$ at small ξ. Remarkably, the stress singularity at the crack tip disappears for any nonzero ν. To see this, look at the contribution to the quantity $\bar{\varepsilon}(\xi)-\varepsilon_\infty$ from the first of the two terms on the right-hand side of (3.11). The constant ε_∞ makes no contribution for $\xi<0$. The nonvanishing part for $\xi<0$, say, $\bar{\varepsilon}_1(\xi)-\varepsilon_\infty$, is

$$\bar{\varepsilon}_1(\xi) - \varepsilon_\infty = -\lim_{\epsilon \to +0} \frac{\varepsilon_\infty}{2\pi i} \int \frac{dk}{k - i\epsilon} \hat{Q}^{(-)}(k) e^{ik\xi}$$

$$= -\lim_{\epsilon \to +0} \frac{\varepsilon_\infty}{2\pi i} \int \frac{dk}{k - i\epsilon} \left[1 - \frac{ik}{p_0} \right]$$

$$\times \exp[\Phi^{(-)}(k) - \Phi^{(-)}(0)]$$

$$\times e^{ik\xi} . \tag{4.10}$$

For negative ξ, we must close the contour of integration around the branch cut in the lower half k plane. At $\xi \to -0$, however, we can move the contour everywhere out to infinity keeping only the contribution ε_∞ from the pole at $k = +i\epsilon$. Here (4.8) plays a crucial role; it tells us that the integrand is well behaved at infinity and that we need only compute the coefficient of k^{-1} at large k in order to evaluate the integral. The result is

$$\bar{\varepsilon}_1(-0) = \varepsilon_\infty e^{-\Phi^{(-)}(0)} \left[1 + \frac{p_\infty}{p_0} \right] . \tag{4.11}$$

So long as p_∞ remains finite, that is, so long as v is nonzero in (4.9), this contribution to the stress is nonsingular.

Application of this technique to both terms in (3.11) produces the following expression for the stress just ahead of the crack tip:

$$\bar{\varepsilon}(-0) = \varepsilon_c\{U(+0)\}$$

$$+ (p_0 + p_\infty) \left[\frac{\varepsilon_\infty}{p_0} e^{-\Phi^{(-)}(0)} \right.$$

$$\left. - \int_0^\infty d\xi\, \varepsilon_c\{U(\xi)\} T(\xi) \right]$$

$$+ \int_0^\infty d\xi\, \varepsilon_c'\{U(\xi)\} T(\xi) , \tag{4.12}$$

where

$$T(\xi) = -\int \frac{dk}{2\pi i} \frac{e^{-\Phi^{(-)}(k) - ik\xi}}{k + ip_0} \tag{4.13}$$

and the prime in (4.12) denotes differentiation with respect to ξ. Note that $T(\xi < 0) = 0$, $T(0) = 1$, and that $T(\xi)$ vanishes as $e^{-\xi}$ for large, positive ξ. Thus the remaining integrations in (4.12), which contain the cohesive stress $\varepsilon_c\{U(\xi)\}$ via the factor $\hat{\Lambda}^{(-)}$ in (3.11), cannot produce any new divergence.

Ordinarily, in models of this kind, the stress ahead of the crack tip has a $1/\sqrt{\xi}$ divergence unless $\varepsilon_c\{U(\xi)\}$ satisfies the so-called "Barenblatt" condition; conversely, the condition that the stress be nonsingular provides important information about $U(\xi)$. That is clearly not the case here. The analogous information in this version of the problem is obtained by looking at $U(\xi)$ near $\xi = +0$. Using methods directly analogous to those described in the preceding paragraphs, it is easy to see that $U'(+0) = 0$ but that $U''(+0)$ does not vanish automatically. The traction on the crack face just behind the tip, that is, the right-hand side of (2.5) evaluated at $\xi \to +0$, is $\varepsilon_c\{U(+0)\} - vU'''(+0)$. If $U''(+0)$ were nonzero, then

$U'''(\xi)$ would have a δ-function singularity at $\xi = 0$. (Remember that $U = 0$ for all $\xi < 0$.) This, in turn, would imply a δ-function singularity in $(\partial u/\partial y)_{y=0}$, which is physically impermissible.

Accordingly, the new Barenblatt condition is $U''(+0) = 0$ which, in the language defined above, turns out to be

$$\varepsilon_\infty = p_0 e^{\Phi^{(-)}(0)} \int_0^\infty d\xi\, \varepsilon_c\{U(\xi)\} T(\xi) . \tag{4.14}$$

We shall see that, in the limit $v \to 0$, the new Barenblatt condition reduces to the old one. Note that (4.14) means that the quantity in square brackets in (4.12) vanishes. Continuing along these lines, with use of (4.14), we find

$$vU'''(+0) = -\int_0^\infty d\xi\, \varepsilon_c'\{U(\xi)\} T(\xi) . \tag{4.15}$$

Thus the combination of (4.12), (4.14), and (4.15) produces

$$\bar{\varepsilon}(-0) = \varepsilon_c\{U(+0)\} - vU'''(+0) , \tag{4.16}$$

which tells us that continuity of stress at the crack tip is automatically assured so long as (4.14) is satisfied.

To complete this section, we need an expression for the crack-opening displacement $U(\xi)$ at arbitrary values of ξ. The algebra required for evaluating (3.10) is lengthy and not at all instructive; as in previous papers in this series, we prefer just to state the result. The form that seems most compact and convenient is

$$U'(\xi) = -\frac{1}{v} \int_0^\xi d\xi'\, S(\xi - \xi') \int_{\xi'}^\infty d\xi''\, T(\xi'' - \xi') \varepsilon_c'\{U(\xi'')\} . \tag{4.17}$$

Here, $T(\xi)$ is the function defined in (4.13), and

$$S(\xi) = -\int \frac{dk}{2\pi} \frac{e^{-\Phi^{(+)}(k) + ik\xi}}{(k - k_1)(k - k_2)} . \tag{4.18}$$

Note that $S(0) = 0$ and $S'(+0) = 1$. Note also that, because of these properties of S, and because the Barenblatt condition (4.14) has been used explicitly in the derivation of (4.17), $U''(+0) = 0$ is satisfied automatically in the latter equation.

V. SPECIFIC RESULTS

Up to this point, we have made no use of the special form of the cohesive stress shown in (2.3), and we have made no approximations whatsoever. Further progress requires both specialization and approximation but, as we shall see, remarkably little loss of generality.

The velocity selection problem is contained in the pair of equations (4.14) and (4.17). The latter is a nonlinear integral equation for $U(\xi)$ that presumably has solutions for arbitrary values of the propagation speed v and the driving force ε_∞. The new Barenblatt condition (4.14) is the single extra condition that is needed to determine v as a function of ε_∞.

The special choice of the cohesive stress shown in (2.3) converts (4.17) from an integral equation to an explicit formula for $U'(\xi)$. Define λ to be the value of ξ such that $U(\lambda) = \delta/W$. Then, on the right-hand side of (4.17),

$\varepsilon_c'\{U(\xi)\}=-\varepsilon_y\delta(\xi-\lambda)$, where $\varepsilon_y=\sigma_y/\mu$ is the yield strain. After one integration over ξ and some minor rearrangement, (4.17) provides the relationship

$$U(\lambda)=\frac{\delta}{W}=\frac{\varepsilon_y}{v}\int_0^\lambda d\xi\, T(\xi)\int_0^\xi d\xi'\,S(\xi')\ ,\qquad (5.1)$$

and (4.14) becomes

$$\varepsilon_\infty=\varepsilon_y p_0 e^{\Phi^{(-)}(0)}\int_0^\lambda d\xi\, T(\xi)\ .\qquad (5.2)$$

We now must evaluate the functions $T(\xi)$ and $S(\xi)$. For $T(\xi)$, we close the contour of integration in (4.13) in the lower half plane to find

$$T(\xi)=e^{-R(p_0)-p_0\xi}+\int_1^\infty\frac{du}{\pi}\frac{e^{-R(u)-u\xi}}{(u-p_0)}\sin\theta(u)\ ,\qquad (5.3)$$

where

$$R(u)=\mathrm{P}\int_1^\infty\frac{dp}{\pi}\frac{\theta(p)}{p-u}\ ,\qquad (5.4)$$

and $\theta(p)$ is defined in (4.5). P denotes a principal-value integration. Similarly, $S(\xi)$ is obtained by closing the contour in (4.18) in the upper half plane:

$$S(\xi)=\frac{\mathrm{Im}[e^{-\Phi^{(+)}(k_1)+ik_1\xi}]}{\mathrm{Re}\,k_1}$$
$$+\int_1^\infty\frac{du}{\pi}\frac{e^{R(u)-u\xi}}{(u+ik_1)(u-ik_1^*)}\sin\theta(u)\ .\qquad (5.5)$$

As argued previously, $\bar\eta$ is an intrinsically small parameter and, therefore, $v\ll 1$ except for values of v very close to unity. In the small-v limit, we can make the approximation

$$\theta(p)\approx\begin{cases}\pi/2 & \text{if }1<p<1/\sqrt{v}\\ 0 & \text{otherwise}\ .\end{cases}\qquad (5.6)$$

Approximations for p_0 and k_1 in this limit are shown in (4.1) and (4.2). Using (5.6), we find

$$R(u)\approx\tfrac{1}{2}\ln\left|\frac{1/\sqrt{v}-u}{u-1}\right|\ ,\qquad (5.7)$$

$$R(0)=\Phi^{(-)}(0)\approx-\tfrac{1}{4}\ln v\ ,\qquad (5.8)$$

$$R(p_0)\approx\tfrac{1}{2}\ln\left[\frac{2}{v^{5/2}}\right]\ .\qquad (5.9)$$

With these approximations in (5.3), a short calculation yields

$$T(\xi)\approx\begin{cases}1 & \text{for }\xi\ll\sqrt{v}\\ \left[\dfrac{\sqrt{v}}{\pi\xi}\right]^{1/2}e^{-\xi} & \text{for }\xi\gg\sqrt{v}\ .\end{cases}\qquad (5.10)$$

The function $S(\xi)$ is somewhat more complicated. The first term on the right-hand side of (5.5) is simply an underdamped oscillation with k_1-dependent amplitude and phase. This term vanishes exponentially fast outside the region $0<\xi<\sqrt{v}$. The second term is more slowly decaying (for small v) and thus is a good approximation for

the function outside that region. For present purposes, we need to know only that

$$S(\xi)\approx\begin{cases}\xi & \text{for }\xi\ll\sqrt{v}\\ \dfrac{v^{3/4}}{\sqrt{\pi\xi}}e^{-\xi} & \text{for }\xi\gg\sqrt{v}\ .\end{cases}\qquad (5.11)$$

The above analysis makes it clear that our basic equations (5.1) and (5.2) involve three competing length scales on the ξ axis. One of these is $\sqrt{v}=|k_1|^{-1}$. This is a dynamic length that we visualize as being microscopically small; it vanishes when either v or $\bar\eta$ goes to zero. A second scale is λ, the length of the cohesive zone (in units βW), which is also microscopic. The third scale is unity in our notation. Because $x+vt=\beta\xi$, and because we already have scaled x by W, unity is the "relativistic" contraction of the macroscopic length W. We need to understand how these scales compare with one another in various situations.

At the Griffith threshold, where crack propagation first becomes energetically possible, we know that $\sqrt{v}$ vanishes because v is zero, and we also know from the original Barenblatt analysis that λ must remain nonzero. To see how this comes about in the present situation, look first at (5.2) with $v\to 0$. Using (4.1), (5.8), and (5.10), and assuming $\lambda\ll 1$, we find

$$\varepsilon_\infty(v\to 0)=\varepsilon_y\int_0^\lambda\frac{d\xi}{\sqrt{\pi\xi}}e^{-\xi}\approx 2\varepsilon_y\left[\frac{\lambda}{\pi}\right]^{1/2}\ ,\qquad (5.12)$$

which is the usual Barenblatt conditions. [Compare this, for example, to Eq. (4.15) in Ref. [2].] In the same limit, (5.1) becomes

$$\frac{\delta}{W}=\frac{\varepsilon_y}{\pi}\int_0^\lambda\frac{d\xi}{\sqrt{\xi}}e^{-\xi}\int_0^\xi\frac{d\xi'}{\sqrt{\xi'}}e^{-\xi'}\approx\frac{2\varepsilon_y}{\pi}\ .\qquad (5.13)$$

Then, eliminating λ from (5.12) and (5.13), we recover the expected formula for the Griffith threshold ε_G:

$$\varepsilon_G\equiv\varepsilon_\infty(v\to 0)=\left[\frac{2\varepsilon_y\delta}{W}\right]^{1/2}\ .\qquad (5.14)$$

As the applied strain ε_∞ increases beyond ε_G, v increases, and $\sqrt{v}$ grows accordingly. The most interesting behavior of this model occurs when the system parameters are such that there exists a regime where $\lambda\ll\sqrt{v}\ll 1$. In this case, we may evaluate the right-hand sides of (5.1) and (5.2) using the approximations for $S(\xi)$ and $T(\xi)$ in (5.10) and (5.11) that are valid for $\xi\ll\sqrt{v}$. Then (5.1) becomes

$$\frac{\delta}{W}\approx\frac{\varepsilon_y}{v}\int_0^\lambda d\xi\int_0^\xi\xi'd\xi'=\frac{\varepsilon_y\lambda^3}{6v}\ ,\qquad (5.15)$$

and (5.2) is simply

$$\varepsilon_\infty\approx\frac{\varepsilon_y\lambda}{v^{1/4}}\ .\qquad (5.16)$$

Eliminating λ from this pair of equations, we find the remarkable results

$$v \approx \left[\frac{W\varepsilon_y}{6\delta} \right]^4 \left[\frac{\varepsilon_\infty}{\varepsilon_y} \right]^{12} , \tag{5.17}$$

$$\lambda \approx \left[\frac{W\varepsilon_y}{6\delta} \right] \left[\frac{\varepsilon_\infty}{\varepsilon_y} \right]^4 . \tag{5.18}$$

The range of validity of (5.17) and (5.18) is determined self-consistently by using those approximations in the condition $\lambda \ll \sqrt{v} \ll 1$. After minor rearrangement, this double inequality becomes

$$\sqrt{3} \ll \frac{\varepsilon_\infty}{\varepsilon_G} \ll \left[\frac{9\varepsilon_y W}{2\delta} \right]^{1/6} , \tag{5.19}$$

where we have used (5.14) to provide an appropriate scale for ε_∞. Thus (5.17) and (5.18) have a large range of validity whenever the macroscopic length scale W is very large. Note that the requirement $\sqrt{v} \ll 1$ does not necessarily mean that v must be small; the upper bound in (5.19) allows v to be very close to unity for small $\tilde{\eta}$.

VI. SUPERSONIC PROPAGATION

So far, all of our calculations have pertained only to the case where $v < 1$. Mathematically, however, this model does allow cracks to propagate at $v \geq 1$ for large but finite values of the applied stress.

One way to see this is to redo the preceding calculations for the special case $v \to 1$, $\beta \to 0$, $\nu \to \infty$ to obtain the corresponding value of ε_∞. In this limit, the branch cuts in $\hat{Q}(k)$ become irrelevant and the integrations in (5.1) and (5.2) can be performed easily. The result, for large W, is

$$\varepsilon_\infty(v=1) = \left[\frac{9\varepsilon_y W}{2\delta} \right]^{1/6} \varepsilon_G = \left[\frac{6\delta}{\varepsilon_y W} \right]^{1/3} \varepsilon_y . \tag{6.1}$$

This is a large value of the applied strain—it is identical to the upper bound of the range of validity for the "slow" approximation in (5.19)—but it is not so large that it contradicts any of our physical assumptions. In particular, the second expression for $\varepsilon_\infty(v=1)$ shown in (6.1) assures us that this value of ε_∞ is much less than the yield strain ε_y.

Supersonic crack propagation occurs in this model because, via the "mass" in (2.1), the system is connected to an infinitely rigid substrate that transmits forces at infinite speed. This high-strain limit would be physically interesting, for example, for a crack propagating in a soft material that is attached elastically to a very rigid one. In this two-dimensional model, where the crack is embedded in an unbounded elastic medium, we expect some change in the response to applied stress as the crack passes through the sound speed at $v = 1$. At supersonic speeds, the crack emits Čerenkov radiation, i.e., it produces a sonic boom which transports energy out to infinity. This mechanism for energy loss produces extra resistance to crack motion.

The qualitative change in the physical behavior of the model at $v = 1$ corresponds to an equally important change in the mathematics. For $v > 1$, we write

$x + vt = \bar{\beta}\bar{\xi}$, where $\bar{\beta}^2 = v^2 - 1$. The analog of (3.4) is then

$$\hat{Q}(k) = (1-k^2)^{1/2} + i\bar{v}k^3 , \tag{6.2}$$

where $\bar{v} = \tilde{\eta}v/\bar{\beta}^3$. Now the branch points lie at $k = \pm 1$, and it is natural to think of the associated branch cuts as running out to infinity along the positive and negative real axes. The condition that $U(\xi)$ be a real function, plus considerations of causality, require that the branch cuts be displaced slightly into the upper half k plane or, equivalently, that the contour of integration in the k plane pass below these cuts. For v not too much larger than unity, $\hat{Q}(k)$ has three zeros on the physical sheet at, say, $\bar{k}_0 = -i\bar{p}_0$, $\bar{k}_1$, and $\bar{k}_2 = -i\bar{k}_1^*$, where $\bar{p}_0$ is real and positive and both the real and imaginary parts of $\bar{k}_1$ are positive. However, as v grows to a value v_c such that $\bar{v}_c = \tilde{\eta}v_c/\bar{\beta}_c^3 = 2/3\sqrt{3}$, the roots at $\bar{k}_1$ and $\bar{k}_2$ move to the real axis where they merge with complex-conjugate roots from the unphysical sheet. For larger values of v, $\hat{Q}(k)$ has four real roots, all at the edge of the unphysical sheet according to our prescription for placement of the branch cuts.

This new analytic structure in the k plane, where $\bar{k}_0$ is the only root of $\hat{Q}(k)$ lying in the lower half plane, means that the Wiener-Hopf factorization is easier than before. There is no need for the extra Cauchy integrals that we used in Sec. IV, and we can choose

$$\hat{Q}^{(-)}(k) = \left[1 + \frac{k}{i\bar{p}_0} \right] , \tag{6.3}$$

$$\hat{Q}^{(+)}(k) = \frac{\hat{Q}(k)}{(1+k/i\bar{p}_0)} . \tag{6.4}$$

Evaluation of (3.11) for the strain along the $\bar{\xi}$ axis ahead of the crack tip then yields the result that $\bar{\varepsilon}(-|\bar{\xi}|) = \varepsilon_\infty$ everywhere; the supersonic crack tip sends no information ahead of itself. The analog of the Barenblatt condition (4.14) becomes

$$\varepsilon_\infty = \bar{p}_0 \int_0^\infty d\bar{\xi} \varepsilon_c \{ U(\bar{\xi}) \} \bar{T}(\bar{\xi}) , \tag{6.5}$$

where

$$\bar{T}(\bar{\xi}) = -\int \frac{dk}{2\pi i} \frac{e^{-ik\bar{\xi}}}{k+i\bar{p}_0} = \begin{cases} e^{-\bar{p}_0\bar{\xi}} , & \bar{\xi} > 0 \\ 0 , & \bar{\xi} < 0 . \end{cases} \tag{6.6}$$

For the crack-opening displacement, in analogy to (4.17), we find

$$U'(\bar{\xi}) = -\frac{1}{\bar{v}} \int_0^{\bar{\xi}} d\bar{\xi}' \bar{S}(\bar{\xi} - \bar{\xi}') \int_{\bar{\xi}'}^\infty d\bar{\xi}'' \bar{T}(\bar{\xi}'' - \bar{\xi}') \times \varepsilon_c' \{ U(\bar{\xi}'') \} , \tag{6.7}$$

where

$$\bar{S}(\bar{\xi}) = \bar{v} \int \frac{dk}{2\pi i} \frac{(k+i\bar{p}_0)}{\hat{Q}(k)} e^{ik\bar{\xi}} . \tag{6.8}$$

The functions $\bar{T}(\bar{\xi})$ and $\bar{S}(\bar{\xi})$ have been normalized so that $\bar{T}(+0) = 1$, $\bar{S}(0) = 0$, and $\bar{S}'(+0) = 1$.

With the special cohesive stress (2.3), the analogs of (5.1) and (5.2) become

$$U(\bar{\lambda})=\frac{\delta}{W}=\frac{\varepsilon_y}{\bar{v}\bar{p}_0}\int_0^{\bar{\lambda}}d\bar{\xi}\,\bar{S}(\bar{\xi})(e^{-\bar{p}_0\bar{\xi}}-e^{-\bar{p}_0\bar{\lambda}}) \qquad (6.9)$$

and

$$\varepsilon_\infty=\varepsilon_y(1-e^{-\bar{p}_0\bar{\lambda}}) \ . \qquad (6.10)$$

For large W and v not too close to unity, it is again appropriate to look at the limit of small $\bar{v}$. In this case, $\bar{p}_0\approx\bar{v}^{-1/2}$. A simple calculation analogous to that leading to (5.17) and (5.18) assumes $\bar{p}_0\bar{\lambda}\approx\bar{\lambda}/\sqrt{\bar{v}}\ll 1$ and yields

$$\frac{1}{\bar{v}}\approx\left[\frac{W\varepsilon_y}{6\delta}\right]^2\left[\frac{\varepsilon_\infty}{\varepsilon_y}\right]^6 , \qquad (6.11)$$

$$\bar{\lambda}\approx\left[\frac{6\delta}{W\varepsilon_y}\right]\left[\frac{\varepsilon_y}{\varepsilon_\infty}\right]^2 . \qquad (6.12)$$

The range of validity for these results, $\bar{\lambda}\ll\sqrt{\bar{v}}\ll 1$, translates into

$$\left[\frac{6\delta}{W\varepsilon_y}\right]^{1/3}\ll\frac{\varepsilon_\infty}{\varepsilon_y}\ll 1 \ . \qquad (6.13)$$

For $v\gg 1$, (6.11) means that

$$v\approx\left[\frac{W\sqrt{\bar{\eta}}\varepsilon_y}{6\delta}\right]\left[\frac{\varepsilon_\infty}{\varepsilon_y}\right]^3 . \qquad (6.14)$$

As ε_∞ approaches ε_y, we see from (6.10) that we must enter a regime in which $\bar{p}_0\bar{\lambda}\approx\bar{\lambda}/\sqrt{\bar{v}}\gg 1$. At $\varepsilon_\infty=\varepsilon_y$, $\bar{\lambda}$ diverges but $\bar{v}$ remains finite; specifically, for large W,

$$\bar{v}(\varepsilon_\infty=\varepsilon_y)=\left[\frac{2\delta}{W\varepsilon_y}\right]^2 . \qquad (6.15)$$

Thus there is an upper limit for the supersonic crack velocities. As we must expect from physical considerations, solutions cease to exist for $\varepsilon_\infty>\varepsilon_y$.

VII. INTERPRETATION AND DISCUSSION

The physical implications of the results for subsonic motion are clearest when they are written in terms of quantities that have the dimensions of stress-intensity factors or, more precisely, strain-intensity factors for simplicity. In particular, we define $K_\infty\equiv\varepsilon_\infty\sqrt{W}$ and $K_G\equiv\varepsilon_G\sqrt{W}=(2\varepsilon_y\delta)^{1/2}$. K_∞ is the appropriate measure of the driving force for crack motion because, via the factor $\sqrt{W}$, it tells us about the concentrated strain in the neighborhood of the crack tip rather than just the strain applied at the distant boundaries. In general, the advantage of writing expressions in terms of the K's is that the dependence—or lack thereof—on the macroscopic length W becomes immediately apparent. As we shall see, the boundaries play a different and more important role in determining the supersonic behavior.

By far the most interesting result to emerge from the preceding analysis is (5.17), which we now write in the form [8]

$$\frac{v}{(1-v^2)^{3/2}}\approx\left[\frac{K_\infty}{K_{\text{eff}}}\right]^{12} , \qquad (7.1)$$

where

$$K_{\text{eff}}=(6\delta)^{1/3}l_\eta^{1/6}\varepsilon_y^{2/3} , \qquad (7.2)$$

and $l_\eta=(c_0\eta/\mu)^{1/2}$ is the length scale that characterizes the viscous force. That is, $\bar{\eta}=(l_\eta/W)^2$. Note further that

$$\frac{K_{\text{eff}}}{K_G}=\left[\frac{9\varepsilon_y l_\eta}{2\delta}\right]^{1/6} , \qquad (7.3)$$

and that K_{eff}, like K_G, is independent of W. In the same spirit, we can use (5.18) to compute the length of the cohesive zone:

$$l_c\equiv\beta W\lambda\approx\left[\frac{2\beta\delta}{3\varepsilon y}\right]\left[\frac{K_\infty}{K_G}\right]^4 . \qquad (7.4)$$

Whenever the right-hand side of (7.3) is appreciably larger than unity, K_{eff} plays the role of an effective Griffith threshold. In that case, the large exponent on the right-hand side of (7.1) implies that v jumps abruptly from very small values to values near unity as K_∞ passes through K_{eff}. The crack makes what would look experimentally like a sharp transition from slow creep at $K_\infty<K_{\text{eff}}$ to propagation at nearly the Rayleigh wave speed for $K_\infty>K_{\text{eff}}$. This effective enhancement of the Griffith threshold depends only on the constitutive properties of the material; the absence of W in (7.2) and (7.3) assures us that the large-scale geometry is playing no role. The cohesive length l_c is also W independent.

An important conclusion from the preceding discussion is that, for subsonic propagation, the speed of the crack and the structure of the cohesive zone are fully determined by the stress-intensity factor K_∞. Although the macroscopic length scale W plays a crucial mathematical role in allowing us to find steady-state solutions, it comes into (7.1) and (7.4) only in the sense that it determines K_∞.

The role of W is very different for supersonic motion. In (6.11) and (6.12), the natural measure of the driving force is the applied strain $\varepsilon_\infty=\Delta/W$ rather than K_∞. The analogs of (7.1) and (7.4) are

$$\frac{(v^2-1)^{3/2}}{v}\approx\left[\frac{l_\eta\varepsilon_y}{6\delta}\right]^2\left[\frac{\varepsilon_\infty}{\varepsilon_y}\right]^6 , \qquad (7.5)$$

$$l_c\approx\left[\frac{6\beta\delta}{\varepsilon_y}\right]\left[\frac{\varepsilon_y}{\varepsilon_\infty}\right]^2 . \qquad (7.6)$$

As mentioned previously, the possibility of supersonic motion is provided by the coupling to infinitely rigid boundaries at distance W, and that situation is reflected in these equations for steady-state response at very large driving force.

To see these properties of the model in more detail, we have solved (5.1) and (5.2) numerically and have computed both v and l_c as functions of the ratio K_∞/K_G or,
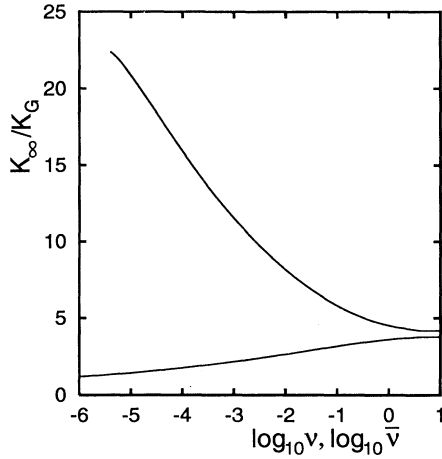
FIG. 1. K_∞/K_G vs $\log_{10}v$ for $v<1$ (lower branch) and K_∞/K_G vs $\log_{10}\bar{v}$ for $v>1$ (upper branch) with $\delta/(W\varepsilon_y)=0.001$.

FIG. 3. v vs K_∞/K_G for $\bar{\eta}=0.00001$ (a), 0.001 (b), and 0.1 (c) with $\delta/(W\varepsilon_y)=0.001$. The dashed lines show the approximation (7.1) for the corresponding parameters.

equivalently for these purposes, as functions of $\varepsilon_\infty/\varepsilon_y$. Our numerical procedure has been to fix the ratio $\delta/(W\varepsilon_y)$, solve (5.1) for λ as a function of v, and then use (5.2) to compute $\varepsilon_\infty/\varepsilon_y$ as a function of v. The latter two functions of v finally can be converted into functions of v for arbitrary values of $\bar{\eta}$, which appears only in the definition of v. Similarly, for $v>1$, we have used (6.9) and (6.10) to compute $\bar{\lambda}$ and $\varepsilon_\infty/\varepsilon_y$ as functions of $\bar{v}$ and then used the definition of $\bar{v}$ to recover the physically meaningful relations between v, l_c, and $\varepsilon_\infty/\varepsilon_y$.

Note that the single system-dependent group of parameters in (5.1) and (5.2), or (6.9) and (6.10), is

$$\frac{\delta}{W\varepsilon_y} = \frac{1}{2}\left[\frac{\varepsilon_G}{\varepsilon_y}\right]^2. \tag{7.7}$$

For any realistic situation, W must be large enough that the yield strain ε_y greatly exceeds the Griffith threshold

ε_G; thus we should use a very small value of $\delta/(W\varepsilon_y)$. Numerical accuracy becomes a problem, however, when the two supposedly microscopic length scales, λ and $\sqrt{v}$, are very much smaller than unity (the macroscopic scale in units βW); but this is what happens—as can be seen by inspection of (5.1) or (6.9)—when $\delta/(W\varepsilon_y)$ is very small. Our numerically feasible compromise has been to use $\delta/(W\varepsilon_y)=0.001$ throughout the computations reported here.

Figures 1 and 2 summarize the initial stage of our numerical analysis; that is, they show K_∞/K_G, λ, and $\bar{\lambda}$ (for $v>1$) as functions of $\log_{10}v$ and $\log_{10}\bar{v}$. In the intermediate range of values of v and $\bar{v}$, the behavior of these functions is qualitatively consistent with (5.17), (5.18), (6.11), and (6.12). Detailed comparisons with these asymptotic estimates are shown in the next three figures.
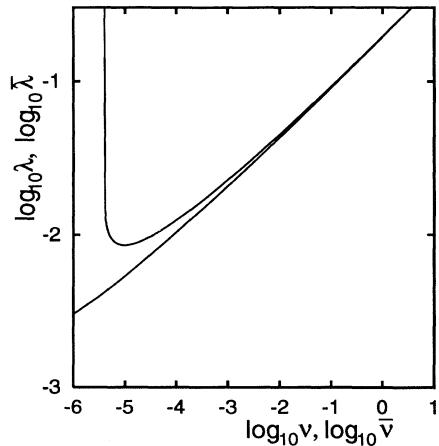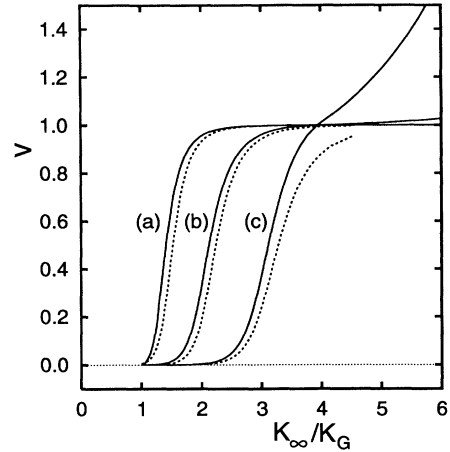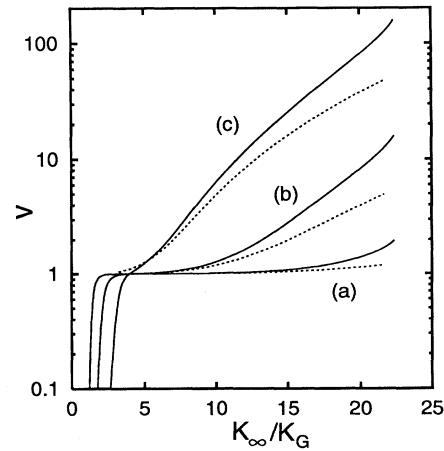
In Fig. 3 we show the velocity v as a function of

FIG. 2. $\log_{10}\lambda$ vs $\log_{10}v$ for $v<1$ (lower branch) and $\log_{10}\bar{\lambda}$ vs $\log_{10}\bar{v}$ for $v>1$ (upper branch) with $\delta/(W\varepsilon_y)=0.001$.

FIG. 4. $\log_{10}v$ vs K_∞/K_G for $\bar{\eta}=0.00001$ (a), 0.001 (b), and 0.1 (c) with $\delta/(W\varepsilon_y)=0.001$. The dashed lines show the approximation (7.5) for the corresponding parameters.
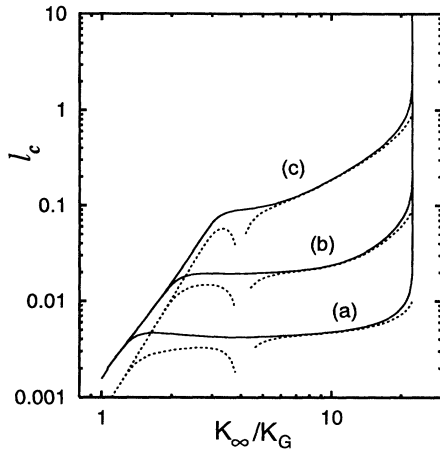
FIG. 5. $\log_{10} l_c$ vs $\log_{10}(K_\infty / K_G)$ for $\tilde{\eta} = 0.00001$ (a), 0.001 (b), and 0.1 (c) with $\delta/(W\varepsilon_y) = 0.001$. The dashed lines show the approximations (7.4) (the left branches for $v < 1$) and (7.6) (the right branches for $v > 1$) for the corresponding parameters.

FIG. 7. U/ε_y vs x in the neighborhood of the cohesive zone. The shaded region indicates the cohesive zone in which $U < \delta/W$. The parameters are $v = 0$ (a), 0.5 (b), 1 (c), and 1.5 (d) with $\tilde{\eta} = 0.001$ and $\delta/(W\varepsilon_y) = 0.001$.

K_∞ / K_G for three values of $\tilde{\eta}$, specifically (a) 0.000 01, (b) 0.001, and (c) 0.1. The values of K_{eff}/K_G for the three cases are (a) 1.557, (b) 2.285, and (c) 3.354. Case (a) is the closest to behaving like a brittle material; K_{eff} is not much greater than K_G and thus v rises rapidly to unity just above the threshold. In cases (b) and (c), the model is behaving in some sense like a ductile material; the onset of rapid fracture does not occur until the applied stress is appreciably greater than the Griffith threshold. In case (c), we have more than a threefold increase in the effective threshold which, according to (5.14), corresponds to a tenfold increase in the effective fracture energy. To achieve this with our relatively large value of $\delta/(W\varepsilon_y)$, however, we have had to use a value of l_η that is not very much less than W. The dashed lines in Fig. 3 show the approximation (7.1) for the corresponding values of $\tilde{\eta}$. This approximation is reasonably
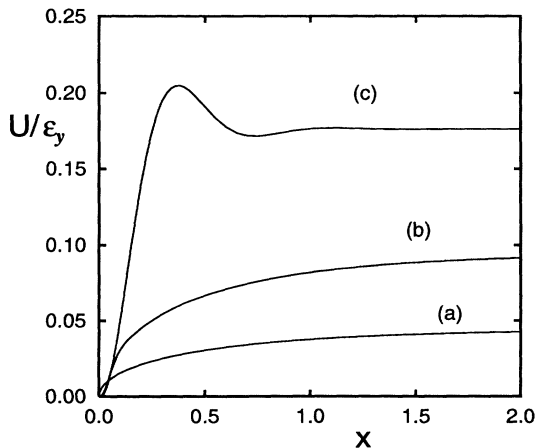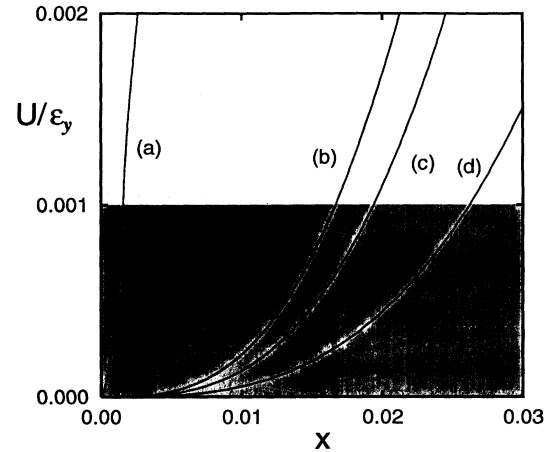
accurate—especially for the smaller values of $\tilde{\eta}$—despite the fact that we are not really probing the asymptotic limit of large W with our choice of system parameters.

The supersonic behavior is illustrated in Fig. 4 in which $\log_{10} v$ is plotted as a function of K_∞ / K_G over the entire range of physically sensible driving forces, $0 < \varepsilon_\infty/\varepsilon_y < 1$ or, equivalently, $0 < K_\infty / K_G < 22.36$. Note that the curves level off above $v = 1$, indicating the onset of radiative energy loss. The effect is least pronounced in case (c) where, presumably, the viscous dissipation remains dominant. The dashed curves are the approximations (7.5) for the corresponding values of $\tilde{\eta}$. As before, agreement with the asymptotic estimates seems reasonable.

Figure 5 is a log-log plot of l_c as a function of K_∞ / K_G, again over the entire range of driving forces, and again for the same three values of $\tilde{\eta}$. Both the subsonic and supersonic approximations for l_c, (7.4) and (7.6), are shown by dashed lines.

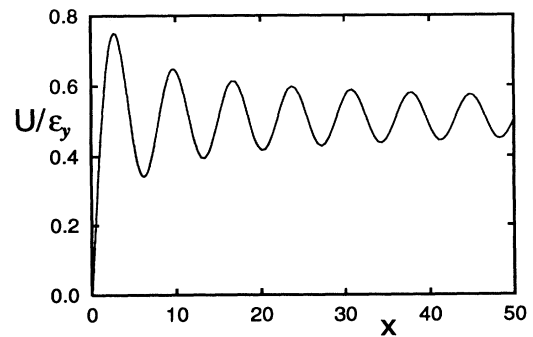The complete crack-opening displacement U as a function of position x can be computed from (4.17) for $v < 1$

FIG. 6. U/ε_y vs x for $v = 0$ (a), 0.5 (b), and 1.0 (c) with $\tilde{\eta} = 0.001$ and $\delta/(W\varepsilon_y) = 0.001$.

FIG. 8. U/ε_y vs x for $v = 1.5$ with $\tilde{\eta} = 0.001$ and $\delta/(W\varepsilon_y) = 0.001$.

and from (6.7) for $v > 1$. In Figs. 6–8, we show U/ε_y as a function of x for $\bar{\eta} = 0.001$ and for various values of v. (Remember that $x = \xi/\beta$ for $v < 1$ and $x = \bar{\xi}/\bar{\beta}$ for $v > 1$.) In Fig. 6, reading from bottom to top, $v = $ (a) 0, (b) 0.5, and (c) 1.0. Both the expected $\sqrt{x}$ near the tip for $v = 0$, and the beginning of an overshoot at $v = 1$, are clearly visible here. The region near the tip is shown in more detail in Fig. 7. Here the values of v, reading from left to right, are $v = $ (a) 0, (b) 0.5, (c) 1.0, and (d) 1.5. At this resolution, we can see clearly that $U \approx x^3$ for $v > 0$. The cohesive zone ends where $U/\varepsilon_y = 0.001$, and the rapid growth of l_c with increasing v is quite visible. Finally, in Fig. 8, we show U for the strongly supersonic case, $v = 1.5$. Here the crack tip is in strong interaction with the rigid "boundaries" implied by finite W, and an underdamped oscillation with wavelength approximately equal to $2\pi v$, that is, with frequency ω_0 in our original notation, has become a pronounced feature of the motion.

ACKNOWLEDGMENTS

[1] M. Barber, J. Donley, and J. S. Langer, Phys. Rev. A **40**, 366 (1989).

[2] J. S. Langer, Phys. Rev. A **46**, 3123 (1992).

[3] Useful general references are M. F. Kanninen and C. H. Popelar, *Advanced Fracture Mechanics* (Oxford University Press, New York, 1985); and L. B. Freund, *Dynamic Fracture Mechanics* (Cambridge University Press, New York, 1990).

[4] A. A. Griffith, Philos. Trans. R. Soc. London, Ser. A **221**, 163 (1920).

[5] J. S. Langer and C. Tang, Phys. Rev. Lett. **67**, 1043 (1991).

[6] G. I. Barenblatt, Adv. Appl. Mech. **7**, 56 (1962). See also D. S. Dugdale, J. Mech. Phys. Solids **8**, 100 (1960) and various discussions of the cohesive zone contained in the books cited in Ref. [3].

[7] C. Myers and J. S. Langer, Phys. Rev. E **47**, 3048 (1993).

[8] An analogous relation can be obtained for the two-dimensional model discussed in Ref. [2]. That model is obtained from this one by adding a viscous term $\eta_b \nabla^2 \dot{u}$ to the right-hand side of the wave equation (2.1) and removing the viscous stress from (2.2). If we define a viscous length l_b by writing $\eta_b = c_0 l_b$, then the analog of (7.1) becomes $v/(1 - v^2)^{3/2} \approx (K_\infty/K_{eff})^4$, where $K_{eff}/K_G = (20\varepsilon_y l_b/\pi\delta)^{1/4}$. For values of the parameters such that K_{eff}/K_G is larger than unity, this model also exhibits a transition between creep and rapidly propagating rupture but, because the exponent is 4 rather than 12, the transition is considerably more gradual than in the model with dissipation on the fracture surface.
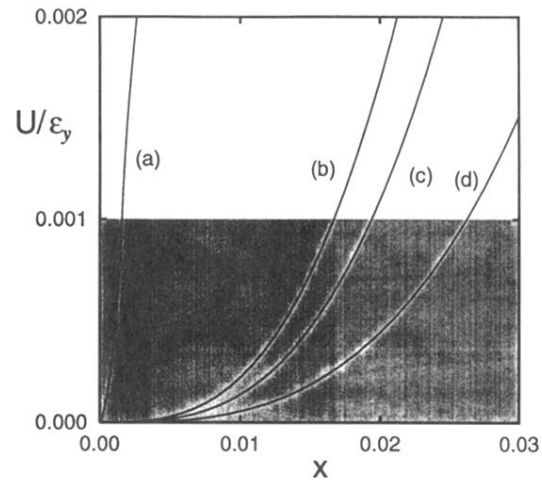
FIG. 7. U/ε_y vs x in the neighborhood of the cohesive zone. The shaded region indicates the cohesive zone in which $U < \delta/W$. The parameters are $v = 0$ (a), 0.5 (b), 1 (c), and 1.5 (d) with $\tilde{\eta} = 0.001$ and $\delta/(W\varepsilon_y) = 0.001$.